Science of the Total Environment 829 (2022) 154729

Contents lists available at ScienceDirect

Science of the Total Environment

journal homepage: www.elsevier.com/locate/scitotenv

Predicting potential wildfire severity across Southern Europe with global data sources

Víctor Fernández-García [a,b,*], David Beltrán-Marcos [a], José Manuel Fernández-Guisuraga [a], Elena Marcos [a], Leonor Calvo [a]

[a] Area of Ecology, Department of Biodiversity and Environmental Management, Faculty of Biological and Environmental Sciences, Universidad de León, 24071 León, Spain
[b] Institute of Geography and Sustainability, Faculty of Geosciences and Environment, Université de Lausanne, Géopolis, CH-1015, Lausanne, Switzerland

HIGHLIGHTS

- State-of-art predictive models of burn severity were developed.
- All climate, topography and fuel characteristics influence burn severity.
- Fuel load variables are the most important when predicting burn severity.
- Multispectral data has higher predictive capacity than radar data.
- Model extrapolation to independent sites implies a decrease in predictive capacity.

GRAPHICAL ABSTRACT

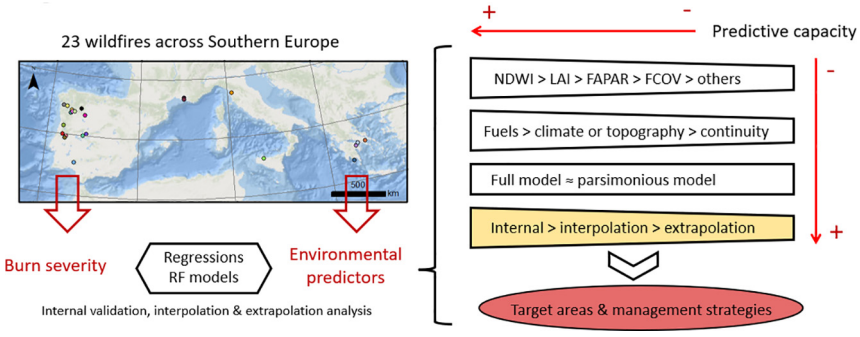

ARTICLE INFO

Article history:
Received 17 January 2022
Received in revised form 17 March 2022
Accepted 17 March 2022
Available online 22 March 2022

Editor: Manuel Esteban Lucas-Borja

Keywords:
Fire severity
Climate
Topography
Fuel load
Fuel moisture
Fuel continuity
Copernicus

ABSTRACT

The large environmental and socioeconomic impacts of wildfires in Southern Europe require the development of efficient generalizable tools for fire danger analysis and proactive environmental management. With this premise, we aimed to study the influence of different environmental variables on burn severity, as well as to develop accurate and generalizable models to predict burn severity. To address these objectives, we selected 23 wildfires (131,490 ha) across Southern Europe. Using satellite imagery and geospatial data available at the planetary scale, we spatialized burn severity as well as 20 pre-burn environmental variables, which were grouped into climatic, topographic, fuel load-type, fuel load-moisture and fuel continuity predictors. We sampled all variables and divided the data into three independent datasets: a training dataset, used to perform univariant regression models, random forest (RF) models by groups of variables, and RF models including all predictors (full and parsimonious models); a second dataset to analyze interpolation capacity within the training wildfires; and a third dataset to study extrapolation capacity to independent wildfires. Results showed that all environmental variables determined burn severity, which increased towards the mildest climatic conditions, sloping terrain, high fuel loads, and coniferous vegetation. In general, the highest predictive and generalization capacities were found for fuel load proxies obtained though multispectral imagery, both in the individual analysis and by groups of variables. The full and parsimonious models outperformed all, the individual models, models by groups, and formerly developed predictive models of burn severity, as they were able to explain up to 95%, 59% and 25% of variance when applied to the training, interpolation and extrapolation datasets respectively. Our study is a benchmark for progress in the prediction of fire danger, provides operational tools for the identification of areas at risk, and sets the basis for the design of pre-burn management actions.

* Corresponding author at: Area of Ecology, Department of Biodiversity and Environmental Management, Faculty of Biological and Environmental Sciences, Universidad de León, 24071 León, Spain.
E-mail address: vferg@unileon.es (V. Fernández-García).

http://dx.doi.org/10.1016/j.scitotenv.2022.154729

1. Introduction

Southern Europe is prone to fire for millennia because of its seasonal climate, characterized by mild winters that promote fuel accumulation, and dry hot summers propitious for fire ignition and spread. Accordingly, fire is considered an integral part of ecosystem dynamics, as well as an evolutionary force in this region (Keeley et al., 2011). However, there are reasons to consider fire as a hazard with negative connotations, and sometimes a disaster because fire can cause losses of human lives, health and human assets (Ribeiro et al., 2020). Also, the large ecological impacts caused by forest fires on vegetation (Fernández-García et al., 2019a, 2020), soil (Pausas et al., 2008; Fernández-García et al., 2019b, 2021), water (Hallema et al., 2018) and fauna (Doherty et al., 2015) can be adverse, particularly in Southern Europe, which is a biodiversity hotspot (Myers et al., 2000) with a high potential erosion risk (Van der Knijff et al., 2000). Moreover, these impacts might be aggravated with the emergence of extreme events, such as the wildfires that occurred in Portugal in 2017, in Greece in 2018 or in Spain in 2012 and 2021, which led to unusual fatalities up to date in Europe (Ribeiro et al., 2020). This new scenario has been attributed to fuel accumulation and landscape homogenization driven by rural depopulation, and to climate change (Pausas et al., 2008; Moreira et al., 2011; Fernández-García et al., 2020). Thus, nowadays the analysis of fire risk related variables is a hot research topic crucial for fire prevention and the design of management strategies (Moreira et al., 2020).

Wildfire danger analysis is usually done on the basis of fire weather indices obtained daily from weather variables at a synoptic level (Jolly et al., 2015; Abatzoglou et al., 2019). These indices, such as the Canadian Fire Weather Index, US Burning Index, or the McArthur Forest Fire Danger Index are mainly related to the ignitability and fire spread rate (Jolly et al., 2015). However, in the current context of change, many experts advocate management aimed at reducing fire damage (or severity), rather than ignition probability or area burned (Moreira et al., 2011; Stephens et al., 2013), because fire-suppression leads to an eventual confluence of extreme fire weather and landscape-scale hazard (Moreira et al., 2020). In this sense, fire research has neglected to develop models that reliably predict landscape-scale susceptibility to severe wildfires. Burn severity, which is inherently linked to variables indicative of the fire harmful power and intensity, can be defined as fire damage on biomass and it is assessed in the field though visual indicators such as char height, degree of vegetation consumption, tree mortality, remaining diameter of branches, litter consumption or ash depth, among others (Keeley, 2009; Key and Benson, 2006). However, the use of field indicators is not functional for the assessment of large areas, and several remote sensing methods have been used to quantify burn severity, including spectral indices (Chu and Guo, 2014; Fernández-García et al., 2018) spectral unmixing analysis (Quintano et al., 2017) or radiative transfer models (Chuvieco et al., 2006; De Santis et al., 2009). Among them, the dNBR spectral index (difference of the Normalized Burn Ratio; López-García and Caselles, 1991), which is based on the sensitivity of near infrared and shortwave infrared reflectance to environmental changes caused by fire (Key and Benson, 2006), is considered the reference metric in Europe, as there, (i) it has shown similar or better relationships with field severity data than other commonly used indices (Gómez-Sánchez et al., 2017; Fernández-García et al., 2018), (ii) it is more consistent among sensors than relativized versions of dNBR such as the RdNBR (Alonso-González and Fernández-García, 2021), and (iii) it is systematically used by the European Forest Fire Information System for post-fire damage assessments (EFFIS) (https://effis.jrc.ec.europa.eu/about-effis) and by the European Emergency Management Service (EMS) (https://emergency.copernicus.eu/).

Identifying the environmental variables that determine burn severity at the landscape scale is essential for the design of management actions aimed at reducing wildfire associated danger (García-Llamas et al., 2019a, 2019b; Moreira et al., 2020), as well as to develop predictive models which serve to identify target areas for pre-fire management and areas where exposure for firefighters during a fire might be unsafe (Connor et al., 2017). In this sense, previous research has differentiated top-down (climate) and bottom-up (topography, fuel load, fuel type, fuel moisture and fuel continuity) drivers of burn severity (Birch et al., 2015; Loehman, 2020). Climate exerts a control of fire regimes through its effects on productivity (and hence fuel load), fuel characteristics (composition, moisture and structure) and fire weather (Walker et al., 2020). Topography determines fire behavior directly, as steep slopes increase propagation rates and flame residence time in upslope fires (Dupuy et al., 2011), but also indirectly, as it conditions mesoscale and microscale climate, airflows (Coen et al., 2013), heat load from solar radiation, and water balances (Kane et al., 2015; Fang et al., 2018). Fuel load and characteristics are probably the primary and major drivers of burn severity (Kalabodikis and Palaiologou, 2019; Walker et al., 2020), flammable vegetation types, high fuel loads and high fuel continuities favouring severe fires. Moreover, fuel moisture, which is closely linked to fire weather, generally decreases wildfire intensity as it increases the energy required for fuel preheating (Lee et al., 2018), and then, during combustion, part of the energy is spent in the heating and evaporation of water (Dillon et al., 2011).

Despite the great relevance of burn severity in fire danger analysis and pre-fire management, most predictive models have been elaborated in individual fire events (e.g. Kane et al., 2015; Fang et al., 2018; García-Llamas et al., 2019a, 2019b; Mitsopoulos et al., 2019). Therefore, inconsistent results have been found between studies, suggesting large site-dependency, and generalization analyses have been bypassed. To address the challenge of elaborating generalizable models applicable at broad scales, the use of global data sources to spatialize both burn severity and its environmental drivers is mandatory. In this way, the multispectral satellite imagery provided by Sentinel-2 since 2015 is an outstanding source to quantify severity at the landscape level because of its spatial (10 m to 60 m), temporal (revisit of 5 days combining 2A and 2B) and spectral resolution (13 bands) (García-Llamas et al., 2019c). Sentinel-2 imagery can also be used to compute spectral indices related to fuel characteristics such as greenness and moisture, and to obtain fuel biophysical properties from radiative transfer models (Pasqualotto et al., 2019; Han et al., 2021). These products also allow to perform second-order textures indicative of fuel continuity (Fernández-Guisuraga et al., 2019). Likewise, the C-band synthetic aperture radar on board Sentinel-1, launched in 2013, periodically retrieves (every 12 days at 5 × 20 m spatial resolution in interferometric wide swath mode) information on surface roughness and dielectric constants, which substantially vary with fuel characteristics and soil moisture (Meyer, 2019; ESA, 2021). This sensor might complement multispectral data not only due to its different sensitivity, but also because of the penetration capacity of C-band pulses in vegetation canopy and soil (Meyer, 2019). In addition, global geospatial products of terrain elevation (SRTM, 2000), climate (Fick and Hijmans, 2017) and land cover (Buchhorn et al., 2020) allow the spatialization of several topographic, climatic and fuel drivers at moderate spatial resolutions worldwide.

The main objective of this study is to analyze the capacity of different environmental variables to predict wildfire severity at the landscape scale across Southern Europe using global data sources. Specifically, we aim to (i) explore the relationship and predictive capacity of individual environmental variables with burn severity, (ii) analyze the relevance of different groups of variables (climatic, topographic, fuel load-type, fuel load- moisture, and fuel continuity) in predicting burn severity, and (iii) to elaborate comprehensive predictive models of burn severity functional over large spatial scales and to analyze for the first time the generalization capacity of predictive models of burn severity.

2. Methods

2.1. Study sites

We selected 23 wildfires that occurred between 2017 and 2020 in Southern Europe: 4 wildfires were located in Portugal, 11 in Spain, 2 in France, 2 in Italy and 4 in Greece (Fig. 1). Burned areas were delimited according to the fire perimeters from the EMS (https://emergency.copernicus.eu/). In the cases where fire perimeters were not available in the EMS, we delineated them over immediate post-fire Sentinel-2 scenes

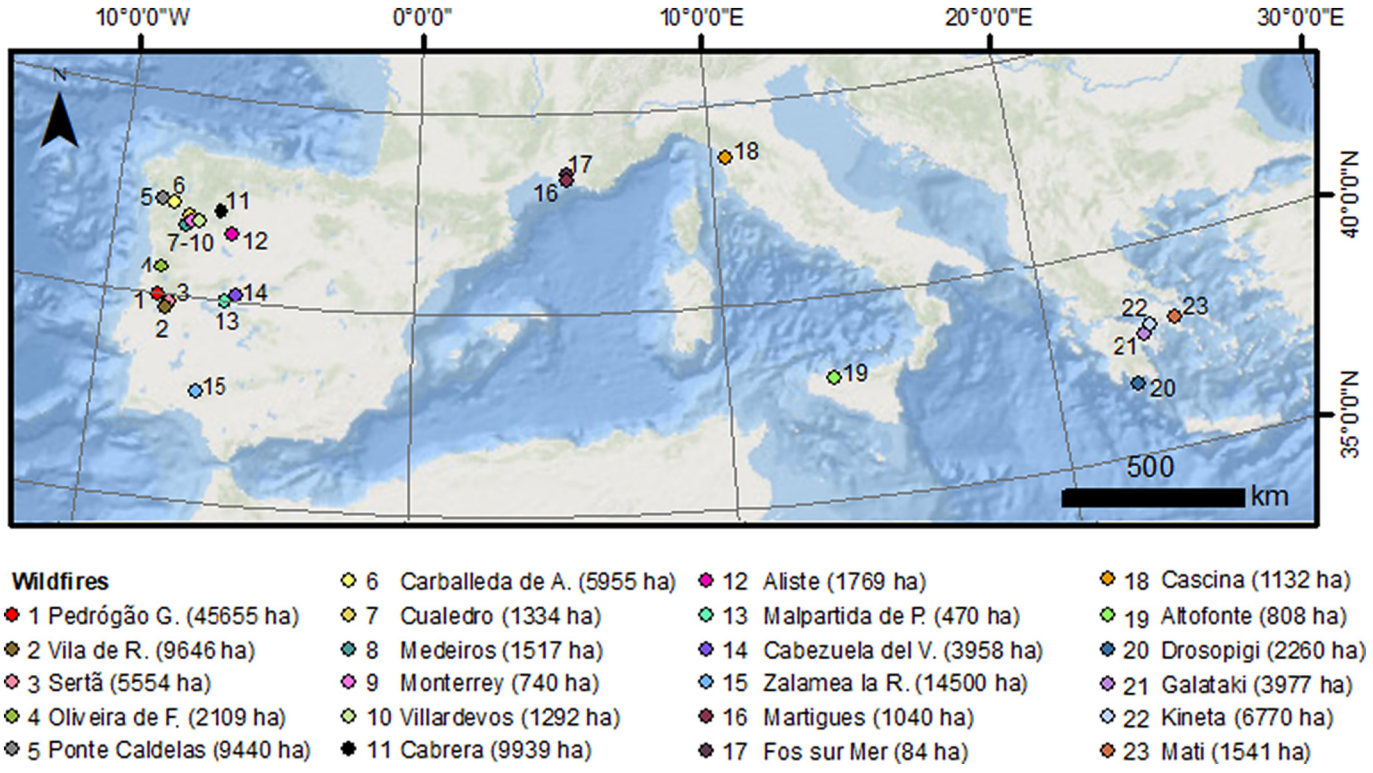

Fig. 1. Map showing the location of the 23 wildfires used in the present study across Southern Europe.

visualized as false colour composites (RGB 547) at a scale of 1:10,000. The selected wildfires reached a total burned area of 131,490 ha, which captures diverse burn severity situations, as well as different topographic, climatic and fuel conditions.

Among the 4 wildfires in Portugal, the wildfire of Predógão Grande was the largest (Table 1). This mega-event started on Jun 2017, burning an area of 45,655 ha, mainly occupied by eucalyptus, pines and mixed forests. In the same region, the wildfire of Vila de Rei burned 9646 ha in July 2019, principally affecting heathlands and coniferous forests. The wildfire of Sertã initiated in July 2020 (5554 ha), burned transitional woodland-shrub ecosystems and heathlands among other land-covers. Two months later, the fire in Oliveira de Frades burned a mosaicked area of 2109 ha composed of coniferous and broadleaved forests, as well as of herbaceous vegetation and crops.

In Spain, the 11 wildfires were selected from North to South, retrieving different climatic conditions (Table 1). In the northwestern part, the wildfire of Ponte Caldelas which started in October 2017, burned 9440 ha of a patchy landscape with broadleaf and mixed forests, heathlands, and spatially complex cultivated areas. In the same month, the wildfire of Carballeda de Avia affected 5955 ha, in this case dominated by heathlands, sparse vegetation and cultivated patches. The wildfires of Cualedro (1334 ha), Medeiros (1517 ha) and Monterrey (740 ha) in summer 2020, mostly

Table 1
Characteristics of the 23 wildfires used in the present study. Annual precipitation and mean annual temperature were averaged for the period 1970–2000 (Fick and Hijmans, 2017).

Study site	Country	Fire alarm date	Annual precipitation (mm)	Men annual temperature (°C)	Elevation range (m)
Predógão Grande	Portugal	17 July 2017	1079	14.3	111–1003
Vila de Rei	Portugal	20 July 2019	877	15.4	144–514
Sertã	Portugal	25 July 2020	1111	13.6	379–1081
Oliveira de Frades	Portugal	7 Sep. 2020	1332	13.6	26–765
Ponte Caldelas	Spain	16 Oct. 2017	1763	13.0	21–729
Carballeda de Avia	Spain	17 Oct. 2017	1610	12.27	234–987
Cualedro	Spain	13 Sep. 2020	1445	11.2	682–933
Medeiros	Spain	30 July 2020	1627	12.3	512–756
Monterrey	Spain	24 July 2020	1647	12.3	405–766
Villardevos	Spain	3 Aug. 2017	1516	11.9	455–922
Cabrera	Spain	21 Aug.2017	1102	8.5	849–1958
Aliste	Spain	15 Aug. 2020	808	11.8	693–1600
Malpartida de Plasencia	Spain	3 Aug. 2020	601	15.0	342–636
Cabezuela del Valle	Spain	28 Aug. 2020	904	10.4	630–1808
Zalamea la Real	Spain	27 Aug. 2020	546	16.8	94–472
Martigues	France	4 Aug. 2020	630	14.9	5–143
Fos sur Mer	France	4 Aug. 2020	641	15.0	6–62
Cascina	Italy	24 Sep. 2018	1093	13.3	7–680
Altofonte	Italy	30 Aug. 2020	572	13.5	498–1141
Drosopigi	Greece	22 Aug. 2020	651	16.2	31–772
Galataki	Greece	25 July 2020	597	15.5	28–789
Kineta	Greece	23 July 2018	593	14.8	7–1326
Mati	Greece	23 July 2018	433	17.4	13–335

burned heathlands and natural vegetation amidst cultivated areas. The Villardevos wildfire in August 2017 burned 1292 ha of heathlands, transitional woodland-shrubs, as well as mixed and coniferous forest. In the Iberian Northern Plateau, the Cabrera wildfire affected 9939 ha in August 2017, mainly occupied by shrubs, herbaceous vegetation and deciduous forest; and the Aliste wildfire in August 2020 burned sclerophyllous vegetation and agricultural areas interspersed with natural vegetation. In the central region, the Malpartida de Plasencia (470 ha) and Cabezuela del Valle (3958 ha) wildfires, which started in August 2020, were selected. Both study sites are dominated by shlerophyllous and herbaceous vegetation. The southernmost wildfire in the Iberian Peninsula was Zalamea la Real in August 2020 that reached 14,500 ha mainly affecting transitional woodland-shrubs, pines and eucalyptus.

In France, two wildfires in the Bouches-du-Rhône department were selected. The Martigues wildfire (1040 ha) started in August 2020, and affected coniferous and schlerophyllous vegetation as well as cultivated areas, whereas the Fos sur Mer wildfire (84 ha), initiated the same day, burned coniferous vegetation.

In Italy we selected the wildfire that occurred in September 2018 in Cascina (1132 ha), Tuscany, in an area occupied by coniferous forests, transitional woodland-shrubs and olive groves; and we selected a second wildfire in Altofonte (808 ha), in August 2020 in Sicily, in an area dominated by coniferous forests.

In Greece we selected two wildfires in the Peloponnese from summer 2020 and two wildfires in Attica from July 2018. In the Peloponesse, the Drosopigi wildfire reached an extent of 2260 ha, burning sclerophyllous vegetation, transitional woodland-shrub, and pastures, whereas the Galataki wildfire (3977 ha) damaged principally coniferous forests and olive groves. In Attica, the Kineta wildfire (6770 ha) combusted coniferous forests and transitional woodland-shrubs, whereas the Mati wildfire (1541 ha) damaged discontinuous urban areas, coniferous forests and sparse vegetation.

The information of the vegetation communities affected in each wildfire was obtained from the Corine Land Cover project (CLC, 2012, 2018).

2.2. Data sources and processing

In this study we used Sentinel-1 and Sentinel-2 satellite data, global climatic data from the Worldclim version 2.1 database at 30 s (Fick and Hijmans, 2017), the SRTM 1 s (30 m) Global digital elevation model (SRTM, 2000) downloaded from the EarthExplorer of United States Geological Survey (https://earthexplorer.usgs.gov/), and the Copernicus Global Land Cover product from the year 2015 at 100 m spatial resolution (Buchhorn et al., 2020), downloaded from the Copernicus Global Land Service (https://land.copernicus.eu/).

Sentinel-1 Interferometric Wide (IW) swath mode Ground Range Detected (GRD) high resolution Synthetic Aperture Radar (SAR) products at dual polarization (VV + VH) were acquired for all study sites, selecting the closest date prior to the wildfires (Table A1). Sentinel-1 products were downloaded from the Copernicus Open Access Hub and then processed in SNAP according to the proposal by Meyer (2019). The procedure consisted of applying precise orbit files, thermal noise removal to reduce noise effects mainly in the inter-sub-swath texture, a removal of GRD-border noise considering a border margin of 500 pixels, and then applying a calibration to convert digital pixel values to radiometrically calibrated SAR backscatter. Our calibrated products were beta0 VV and VH backscatter bands, which were subsequently multilocked to 20 m square pixels. Then, we reduced speckle effects by applying a refined Lee filter, and we applied a terrain flattening correction using the SRTM digital elevation model. Finally, we implemented a range doppler terrain correction using the SRTM digital elevation model, obtaining gamma0 radar backscatter products. Finally, we converted the unitless gamma0 backscatter values to dB units using a logarithmic transformation.

Pre- and post-burn Sentinel-2 level 1C images were selected for each study wildfire (Table A1). The closest images to the date of the fire event, and free of clouds, were selected by visually checking the scenes in the Sentinel Hub EO Browser (https://apps.sentinel-hub.com/eo-browser/), and downloaded from the Copernicus Open Access Hub (https://scihub.copernicus.eu/). Then, we used the Sen2Cor 280 processor with the SRTM digital elevation model to obtain topographically and atmospherically corrected Sentinel-2 level 2A images. The 10 m resolution bands of Sentinel-2 level 2A images were downsampled to 20 m spatial resolution aggregating the pixels to the mean value. Moreover, in the cases where more than one Sentinel-2 scene was necessary to capture the entire study wildfire, we mosaicked the contemporary scenes using the SNAP mosaicking tool.

2.3. Burn severity

We assessed burn severity using pre- and post-fire Sentinel-2 processed images through the dNBR index (López-García and Caselles, 1991), which is commonly used by public organisms and programs of the European Union and United States of America (Fernández-García et al., 2021), and its performance has been largely validated with field data or through photointerpretation in Southern Europe (e.g. Veraverbeke et al., 2010; Fernández-García et al., 2018), including several of our study sites (García-Llamas et al., 2019b; Fernández-Manso et al., 2020).

The calculation of dNBR comprises two steps, first the Normalized Burn Ratio (NBR) is calculated for the pre- and post-fire according to the Eq. (1), and second, the pre- and post-burn values are differenced according to Eq. (2). NBR values are usually multiplied by 1000 (see Eq. (1)), and consequently dNBR values range between −2000 and 2000. dNBR values increase proportionally to burn severity, usually up to 1200 in the most severely burned areas, whereas unburned or slightly burned areas show dNBR values close to 0.

$$NBR = \frac{(\rho 8a - \rho 12)}{(\rho 8a + \rho 12)} \times 1000 \quad (1)$$

Where NBR is the Normalized Burn Ratio, and ρ8a and ρ12 are the reflectance values of bands 8a (near infrared) and 12 (shortwave infrared) from Sentinel-2 level 2A images.

$$dNBR = preNBR - postNBR \quad (2)$$

where dNBR is the difference of the Normalized Burn Ratio, and preNBR and postNBR are the Normalized Burn Ratio indices calculated for the pre-burn and post-burn scenes, respectively.

2.4. Environmental predictors

We generated a set of 20 environmental variables to predict burn severity across Southern Europe, which were classified into five groups: climatic, topographic, fuel load-type, fuel load-moisture and fuel continuity variables (Table 2).

Five climatic variables averaged for the period 1970–2000 were directly acquired from the Worldclim database (Fick and Hijmans, 2017): mean annual temperature (MAT), annual precipitation (AP), precipitation seasonality (PS) calculated through the coefficient of variation of the mean monthly temperatures, mean temperature of the driest quarter (MTDQ), and the precipitation of the driest quarter (PDQ). Moreover, we computed temperature seasonality as the coefficient of variation of the mean monthly temperatures, using the temperature seasonality product (standard deviation) and MAT from the Worldclim database.

We used four topographic variables geo-processed in ArcMap 10.7 (ESRI, 2019) from the SRTM 1 s Global digital elevation model: slope, topographic position index (TPI), topographic convergence index (TCI), and heat load (HL). TPI, TCI and HL were computed using the topography tools 10.3 toolbox (Dilts, 2015). The TPI was calculated according to Jenness (2006), comparing the elevation of each pixel to the mean elevation of its 24 neighbor pixels (25 m kernel). This algorithm results in negative values in ridge areas or mountain tops, and positive values in valleys or

Table 2
Environmental variables and groups used as predictors of burn severity. The table also shows the abbreviations, units and data sources for each variable, and processing applied after data acquisition.

Group	Environmental variable	Abbreviation	Units	Data source	Processing
Climatic	Mean annual temperature	MAT	°C	Worldclim	No
	Annual precipitation	AP	mm	Worldclim	No
	Temperature seasonality	TS	–	Worldclim	Yes
	Precipitation seasonality	PS	–	Worldclim	No
	Mean temperature of driest quarter	MTDQ	°C	Worldclim	No
	Precipitation of driest quarter	PDQ	mm	Worldclim	No
Topographic	Slope	Slope	°	SRTM	Yes
	Topographic position index	TPI	–	SRTM	Yes
	Topographic convergence index	TCI	–	SRTM	Yes
	Heat load	HL	MJ cm^{-2} $year^{-1}$	SRTM	Yes
Fuel load-type	Copernicus global land cover class	GLC class	–	GLC 2015	No
	Pre-burn fraction of absorbed photosynthetically active radiation	FAPAR	–	Sentinel-2	Yes
	Pre-burn leaf area index	LAI	m^2 m^{-2}	Sentinel-2	Yes
	Pre-burn fraction of vegetation cover	FCOV	–	Sentinel-2	Yes
Fuel load-moisture	Pre-burn normalized difference water index	NDWI	–	Sentinel-2	Yes
	Pre-burn moisture stress index	MSI	–	Sentinel-2	Yes
	Pre-burn canopy water content	CWC	g m^{-2}	Sentinel-2	Yes
	Pre-burn C-band synthetic aperture radar cross ratio	CR	–	Sentinel-1	Yes
Fuel continuity	Pre-burn global land cover patch size	Patch size	ha	GLC 2015	Yes
	Homogeneity of pre-burn FCOV	FCOV homogeneity	–	Sentinel-2	Yes

cliff bases. The TCI, also known as the topographic wetness index, is a hydrological-based topographic index that describes the tendency of an area to retain or evacuate water under stable conditions, values increasing from 0 proportionally to the topographic water retention proneness. It was computed considering the contributing areas determined according to the model proposed by Tarboton (1997), and the slope of the digital elevation model. Finally, the HL was calculated according to the proposal of McCune and Keon (2002), using slope, aspect, and latitude to estimate the potential annual direct incident radiation, which usually ranges between 0 and 1.1 MJ * cm^{-2} yr^{-1} in southern European latitudes.

The four predictors applied as proxies of fuel load-type included a categorical variable (pre-burn land cover classification) and three continuous biophysical variables (the pre-burn fraction of absorbed photosynthetically active radiation, FAPAR; the pre-burn leaf area index, LAI; and the pre-burn fraction of vegetation cover, FCOV). In relation to the first, we used the land cover classification from the Copernicus Global Land Cover (GLC class) of the year 2015, which differentiates 22 land cover classes, 13 of them being frequent in terrestrial ecosystems of Southern Europe. Moreover, the three biophysical variables (FAPAR, LAI and FCOV) were computed from pre-processed Sentinel-2 images (see Section 2.2) using the biophysical processor embedded in SNAP. This processor retrieves the biophysical parameters by applying an artificial neural network pre-trained with a database (lookup-table) generated using a radiative transfer model (RTM) based on PROSAIL (Weiss and Baret, 2016). Moreover, the biophysical processor presumes to be applicable to any type of vegetation with reasonable performances, as the RTM is configured to accurately simulate the canopy reflectance as observed within Sentinel-2 bands and geometry over most vegetation types and conditions across the globe (Xie et al., 2019).

Four variables directly related to fuel load-moisture, and indirectly to fire weather, were studied, including two spectral indices (pre-burn normalized difference water index, NDWI; and pre-burn moisture stress index, MSI), one biophysical variable (pre-burn canopy water content, CWC) and the pre-burn C-band synthetic aperture radar cross ratio (CR). The NDWI (Eq. (3)) and MSI (ratio between band 11 and band 8) were calculated from Sentinel-2 pre-processed images (see Section 2.2). NDWI and MSI indices are closely related to living vegetation moisture and dead fuel moisture respectively (Babu et al., 2015), also being linked to fuel load, the lowest values indicating high living fuel loads and water contents, and the highest values indicating low living fuel load and dry conditions. Likewise, the CWC was computed from pre-processed Sentinel-2 images, using the biophysical processor in SNAP. The CR was obtained from Sentinel-1 IW GRD dual polarization (VV + VH) pre-processed images, as the ratio between VH backscatter and VV backscatter. Radar backscatter depends on terrain structure, surface roughness and dielectric constant of the materials on the ground, which is principally influenced by vegetation and water content (Vreugdenhil et al., 2018; ESA, 2021).

$$NDWI = \frac{(\rho 3 - \rho 8)}{(\rho 3 + \rho 8)} \quad (3)$$

where NDWI is the Normalized Difference Water Index, and ρ3 and ρ8 are the reflectance values of bands 3 (green) and 8 (near infrared) from Sentinel-2 pre-processed images.

Fuel continuity was measured using two different approaches: pre-burn global land cover patch size (patch size) and homogeneity of pre-burn FCOV (FCOV homogeneity). Patch sizes were calculated from the Copernicus Global Land Cover product of the year 2015 considering all classes, as the hectares occupied by each patch. On the contrary, FCOV homogeneity was calculated from the FCOV biophysical variable using the ENVI 5.3 program (Exelis Visual Information Solutions, 2015). FCOV homogeneity is a second-order texture that was computed using a 64-level co-occurrence matrix. The analysis was performed using a kernel of 5 × 5 pixels, moving in four directions (0°, 45°, 90° and 135°). Then, the values obtained for the four directions were averaged to obtain a directionally invariant FCOV homogeneity (Fernández-Guisuraga et al., 2019), with values ranging from 0 (completely heterogeneous) to 1 (completely homogeneous).

2.5. Data extraction and analysis

Data of burn severity and all environmental predictors was systematically extracted using one sampling point per hectare, with a distance between points fixed to 100 m (5 Sentinel-2 pixels), which is appropriate to avoid spatial autocorrelation in burn severity measured from Sentinel-2 imagery (Fernández-Guisuraga et al., 2021). Then, points were inspected to remove those with anomalous values for some of the studied variables (mostly points with dNBR values lower than −100, which usually corresponded to small, unburned patches within the fire perimeter). The final dataset was configured by the information extracted from 130,378 sampling points, which showed a Moran's *I* value for the response variable (dNBR) of 0.018, corroborating the lack of significant spatial autocorrelation patterns (Moran's $I < 0.1$; Diniz-Filho et al., 2012).

To train predictive models of burn severity, as well as for model interpolation and model extrapolation analysis, we randomly divided our data into three different datasets: (i) The training dataset, which was configured with 80% of the data from the wildfires of Predógão Grande, Vila de Rei, Oliveira de Frades, Ponte Caldelas, Cualedro, Medeiros, Monterrey, Villardevos,

Cabrera, Aliste, Malpartida de Plasencia, Cabezuela del Valle, Zalamea la Real, Martigues, Cascina, Altofonte, Drosopigi, Kineta and Mati (n = 90,501). (ii) The dataset for model interpolation analysis, which was configured with the remaining 20% of data from these wildfires (n = 22,624). (iii) The dataset for model extrapolation analysis, which was conformed with the data extracted from the Sertã, Carballeda de Avia, Fos sur Mer and Galataki wildfires (n = 17,253).

We studied the relationship between individual environmental variables (predictors; Table 2) and burn severity (response variable) through univariant models using the *lm* function. For the continuous environmental variables, we performed models with linear, quadratic and cubic predictor terms using the training dataset, and we selected the model with the lowest Akaike information criterion (AIC) value, as long as it also met the requirement of having the lowest AIC when applied to the datasets for model interpolation and extrapolation analysis. These criteria allowed non-overfitted and generalizable relationships between each environmental variable and burn severity to be obtained.

We analyzed the relevance of different groups of variables (Table 2) in predicting burn severity through five different random forest (RF) models. The predictors of each random forest model were all the variables of each group.

In order to obtain the most effective and efficient models to predict burn severity across southern Europe, we elaborated a full RF model and a parsimonious RF model, respectively. The full model included all environmental predictors used in the present study (Table 2). On the contrary, the parsimonious model was obtained by reducing the full model following two steps. Firstly, we assessed collinearity among predictors with the Pearson's correlation coefficient (*cor.test* function, for pairs of continuous variables), or with the coefficient of determination (R^2) of univariant models (*lm* function, for pairs of the categorical variable and each continuous variable). In the case of correlation (Pearson's $R > |0.7|$ or $R^2 > 0.49$) we retained from each pair of predictors, the most related to burn severity according to the goodness-of-fit of the linear models explained in the previous paragraphs. Secondly, we performed a recursive feature elimination with the *rfe* function, using 10-fold cross-validation and 5 repeats to improve the performance of feature selection, partitioning the dataset into 80% (training) and 20% of data (validation). The importance of the retained predictors in the parsimonious model was assessed by the percentage increase in mean square error (%IncMSE) when this variable is randomly permuted, using the *importance* function.

All RF models were implemented with the *randomForest* function using the training dataset. The ntree parameter ntree (number of trees grown) was fixed to 1000, which guarantees the quality and stability of results according to mean out-of-bag error curves, and is both a large and a computationally feasible value for our datasets (Probst and Boulesteix, 2018); and mtry (number of predictors sampled for spliting at each node) was fixed to one third of the number of predictors, the default option that was consistent with the results of 10-fold cross validations performed with the functions *trainControl* and *train*.

The trained models (univariant regressions and RF models) were applied to the three datasets for internal validation, model interpolation and model extrapolation analysis. Model fitting and predictive capacity was assessed with the normalized root-mean square error (nRMSE), which was calculated in percentage by dividing the RMSE measured in dNBR units per the dNBR range ($dNBR_{max}$- $dNBR_{min}$) of our entire dataset, and multiplying the result per 100. The proportion of variance explained by the models (R^2) was also shown.

All statistical analyses were performed in R (R Core Team, 2021), using *randomForest* (Liaw and Wiener, 2002) and *caret* (Kuhn, 2008) packages.

3. Results

3.1. Individual environmental variables: relationship with burn severity and predictive capacity

The univariant models showed that all the studied environmental variables were significantly related to burn severity ($P < 0.01$; Table A2). Focusing on continuous environmental variables (Fig. 2), most models were better fitted when using cubic predictors (PDQ, Slope, HL, FAPAR, LAI, FCOV, NDWI and MSI models) or quadratic predictors (MAT, AP, TS, PS, TCI, CR and Patch size models models), whereas only four variables were better fitted using linear predictors (MTDQ, TPI, CWC and FCOV homogeneity) according to AIC (Table A2).

In general, nRMSE values of the models ranged from 14.65 to 17.80 (and R^2 values from 0.33 to 0.00), revealing large differences depending on the environmental predictor (Fig. 2; Fig. 3). The environmental variable that showed the strongest relationship with burn severity was the pre-burn NDWI index (using a cubic predictor), with an nRMSE value of 14.65 (R^2 = 0.33). The cubic relationship (Fig. 2) showed that neither the lowest (high fuel load and water content) nor the highest (low fuel load and water content) NDWI values were associated to the highest severities, and an inverse relationship with burn severity was found at the intermediate NDWI range (i.e., at intermediate fuel load and water content). The model based on NDWI also showed the highest predictive capacity when applied to independent points within the training wildfires (interpolation) (nRMSE = 14.69; R^2 = 0.32), as well as when extrapolating model predictions to different wildfires (nRMSE = 15.71; R^2 = 0.23) (Table 3).

The predictors that showed the strongest relationships with burn severity after NDWI, were the vegetation biophysical variables FAPAR, LAI and FCOV (cubic predictors) (Fig. 2). These variables were positively related to burn severity at low and intermediate values (i.e., low and intermediate vegetated areas), with nRMSE values ranging from 15.07 to 15.27 (R^2 = 0.27 to 0.29). The models performed with these variables differed in their predictive capacity when applied to independent data (Table 3), the FAPAR model showing the highest extrapolation capacity (nRMSE = 16.10; R^2 = 0.19).

Following a decreasing order, the fuel load-moisture variables MSI and CWC (cubic and linear predictors) reached the next strongest relationship with burn severity, with nRMSE values of 15.75 and 16.35, respectively (R^2 = 0.22 and 016) (Fig. 2). MSI decreased with burn severity except at high MSI values (i.e., except at higher water stress and less water content). On the contrary, CWC increased with burn severity. The model based on MSI showed a higher interpolation (nRMSE = 15.74; R^2 = 0.22) and extrapolation (nRMSE = 16.85; R^2 = 0.12) capacity than the model based on CWC (Table 3).

The AP (quadratic predictor) and PDQ (cubic predictor) were the climatic variables that showed the strongest relationship with burn severity (nRMSE = 16.72 and 16.88; R^2 = 0.12 and 0.10 respectively) (Fig. 2), being low annual precipitations and low precipitations in the driest quarter (<50 mm) associated to low severity situations. The interpolation of model predictions showed similar results, but the predictive capacity decreased when applied to independent wildfires (nRMSE ≥17.26; $R^2 \leq 0.08$) (Table 3).

The relationship between the studied categorical environmental variable (land cover class) and burn severity (Fig. 3; nRMSE = 17.03; R^2 = 0.09) showed that closed monotype forests and dense shrublands (GLC classes 111, 126 and 114) are prone to higher severities than open or mixed ones. Additionally, results demonstrate that cultivated and managed vegetation, areas with water bodies or built up, and open deciduous broadleaf forests are associated with the lowest severities. The interpolation of the

Fig. 2. Density scatterplots showing the relationships between burn severity and the different environmental variables (see Table 2 for further details). Red lines represent the best fitted model (linear, quadratic or cubic) selected according to model performance analysis, interpolation and extrapolation capacity. Density was calculated based on two-dimensional kernel density estimations using the *geom_pointdensity* function (Kremer and Anders, 2019).

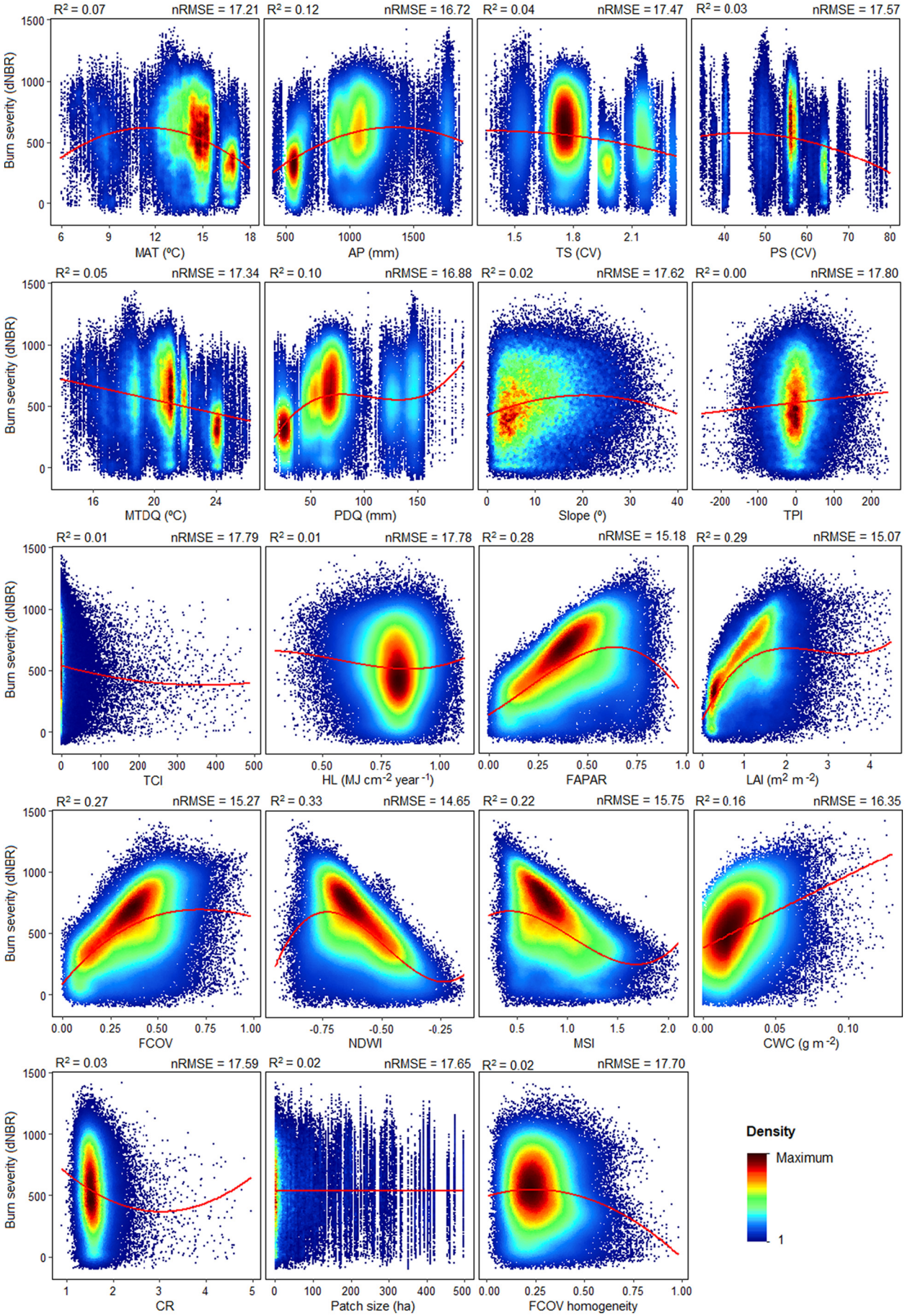
R² = 0.07 nRMSE = 17.21
MAT (ºC)
R² = 0.12 nRMSE = 16.72
AP (mm)
R² = 0.04 nRMSE = 17.47
TS (CV)
R² = 0.03 nRMSE = 17.57
PS (CV)
R² = 0.05 nRMSE = 17.34
MTDQ (ºC)
R² = 0.10 nRMSE = 16.88
PDQ (mm)
R² = 0.02 nRMSE = 17.62
Slope (º)
R² = 0.00 nRMSE = 17.80
TPI
R² = 0.01 nRMSE = 17.79
TCI
R² = 0.01 nRMSE = 17.78
HL (MJ cm-2 year-1)
R² = 0.28 nRMSE = 15.18
FAPAR
R² = 0.29 nRMSE = 15.07
LAI (m2 m-2)
R² = 0.27 nRMSE = 15.27
FCOV
R² = 0.33 nRMSE = 14.65
NDWI
R² = 0.22 nRMSE = 15.75
MSI
R² = 0.16 nRMSE = 16.35
CWC (g m-2)
R² = 0.03 nRMSE = 17.59
CR
R² = 0.02 nRMSE = 17.65
Patch size (ha)
R² = 0.02 nRMSE = 17.70
FCOV homogeneity
Burn severity (dNBR)
Density
Maximum
1

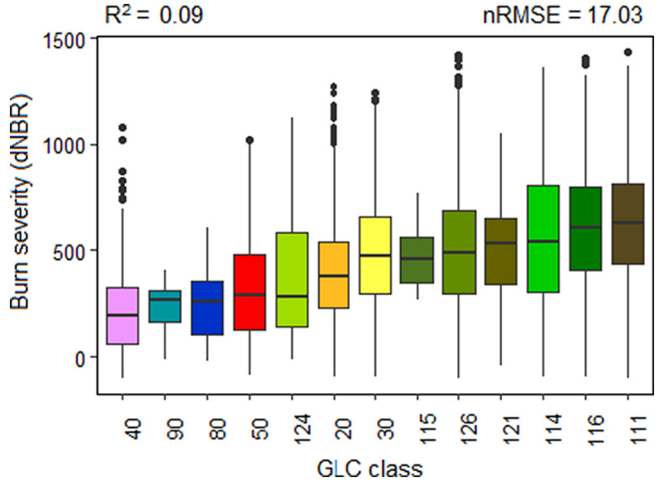

Fig. 3. Boxplot showing the relationship between burn severity and the different pre-burn land cover classes. The plot shows each class using its corresponding Copernicus GLC class colour and code (numbers in the horizontal axis). 40: cultivated and managed vegetation; 90: herbaceous wetland; 80: areas with predominance of permanent water bodies; 50: predominantly built up; 124: open deciduous broadleaf forest; 20: shrubs; 30: herbaceous vegetation; 115: closed mixed forest; 126: open unknown forest, usually including sparse shrublands in our study sites; 121: open evergreen needle leaf forest; 114: closed deciduous broadleaf forest; 116: closed unknown forest, usually including dense shrublands in our study sites; 111: closed evergreen needle leaf forest.

model based on GLC class did not decrease the predictive accuracy (nRMSE = 17.02; R^2 = 0.09), whereas the extrapolation capacity was lower (nRMSE = 18.21; R^2 = 0.03) (Table 3).

The rest of the environmental predictors (MAT, TS, PS, MTDQ, Slope, TPI, TCI, HL, CR, Patch size and FCOV homogeneity) showed weaker relationships with burn severity (nRMSE >17.00 and R^2 < 0.00) (Fig. 2), and their model interpolation and extrapolation capacity was also lower (Table 3).

3.2. Predictive capacity of different groups of environmental variables

In general, the RF models performed by groups of variables (climatic, topographic, fuel load-type, fuel load-moisture, and fuel continuity) showed a better fit to the training data (Table 4) than the univariant models performed with each environmental variable (Fig. 2). In this sense, the nRMSE between observed and predicted values ranged from 8.78 to 13.71 (R^2 values from 0.81 to 0.41). However, the predictive error of all RF models increased when interpolating them, with nRMSE values ranging from 14.14 to 17.43 (R^2 values from 0.05 to 0.37); and even more when extrapolating them, with nRMSE values from 16.16 to 20.52 (R^2 values from 0.00 to 0.22) (Table 4). In this sense, extrapolations based on NDWI (cubic predictor) were more accurate than all the RF models by groups of variables.

Ranking the predictive capacity by groups (Table 4), we found that the fuel load-moisture variables were the most accurate when predicting burn severity in all datasets (training, interpolation and extrapolation) in terms of nRMSE (8.78 to 16.16), followed by fuel load-type (12.07 to 16.17) and topographic variables (11.28 to 17.89). Fuel continuity and climatic variables showed a lower predictive capacity in all datasets than the foregoing.

3.3. Predictive capacity combining all environmental variables

The full RF model showed the highest predictive capacity among all the models in the present study, as shown by the performance metrics obtained when applied to the training (nRMSE = 4.78; R^2 = 0.95), interpolation (nRMSE = 11.51; R^2 = 0.59), and extrapolation datasets (nRMSE = 16.02; R^2 = 0.25) (Fig. 4).

The collinearity analysis to obtain the parsimonious RF model (Fig. A1) showed that most climatic variables were correlated among them, as well as most fuel load-type and fuel load-moisture variables. The result of the removal of collinear variables and the recursive feature elimination was a parsimonious model with 7 predictors, being the most important the NDWI (Fig. 5). Topographical (TPI, Slope), climatic (PDQ and TS), fuel continuity (patch size) and fuel load-type (GLC class) also contributed to enhancing model predictions.

The predictive capacity of the parsimonious RF model was similar to the full RF model (Fig. 6), and its predictive capacity also decreased from the training (nRMSE = 5.85; R^2 = 0.92) to the interpolation (nRMSE = 12.01; R^2 = 0.55) and validation datasets (nRMSE = 15.95; R^2 = 0.24).

4. Discussion

4.1. Relationships between environmental variables and burn severity

Our results confirm that all the studied climatic, topographic, and fuel-related variables were significantly related to burn severity. However, the individual analysis of each predictor revealed that the strongest relationships with burn severity were found for fuel load variables, which is in accordance to previous work (e.g., Birch et al., 2015; García-Llamas et al., 2019a; Walker et al., 2020). Among fuel load-related variables, those computed from Sentinel-2 (FAPAR, LAI, FCOV, NDWI, MSI, CWC) were highly correlated among them (Fig. A1), which can be a consequence of the governance of the amount of living biomass over the remaining fuel biophysical properties. In this sense and focusing on the NDWI as the best related variable to burn severity, we found a clear pattern of increasing severity towards high fuel amounts at intermediate fuel load and moisture conditions. This behavior has been reported in other regions (e.g., Walker et al., 2020; Kraaij et al., 2018), corroborating that fuel amount is a primary driver of burn severity during the fire season in the ecosystems of southern Europe (García-Llamas et al., 2019a, 2019b). However, the cubic relationship between NDWI and burn severity also reveals that both NDWI extremes, represented by very high living biomass-moisture, and very low living biomass-moisture led to low severity values, because flammability limitations and fuel-load limitations respectively. This indicates that key biophysical factors (fuel load and moisture) must coincide for wildfires not only to occur (Krawchuk and Moritz, 2011) but also to be severe, providing evidence of the varying constraints hypothesis in the context of burn severity. In the same way, burn severity varied with land cover classes, maximum severities being reached in closed coniferous forests and shrublands. This can be attributed not only to fuel load and moisture dynamics, but also to the structure and flammability of Mediterranean pines and shrubs, which facilitates severe crown fires more than in other vegetation types (Keeley et al., 2011; Kalabodikis and Palaiologou, 2019). The CR radar metric, which was selected as complementary proxy of fuel load and moisture, significantly decreased as the other fuel load and moisture proxies increased (Fig. A1). The capacity of CR to indicate fuel load and moisture is a consequence of the preference of VV and VH polarizations for different scattering types (rough surface scattering, double bounce scattering and volumetric scattering), which vary with vegetation structure and dielectric properties (Meyer, 2019; Saatchi, 2019). However, the CR relationship with burn severity was weaker than those metrics obtained from Sentinel-2, probably because of the elevated radar noise at spatial scales comparable to Sentinel-2 (Meyer, 2019), and to the effect of soil roughness, which also causes depolarization, roughed soils potentially giving similar backscatter than vegetated areas (Vreugdenhil et al., 2018).

The relationships between burn severity and all climatic variables suggest that the sites with the mildest climates (i.e., high annual rainfall, low summer aridity, intermediate annual temperature, cool summers and low seasonality) are those with the highest severity. This agreed with the results obtained by Parks et al. (2016) in Western US, which suggested that climate effects on burn severity are mediated by climate influence on ecosystem

Table 3
Results of internal validation (fitting of model predictions to the training data), interpolation (fitting of model predictions to independent data within the training wildfires) and extrapolation (fitting of model predictions to data from independent wildfires) of the univariant models performed with each environmental variable. The performance of linear, quadratic and cubic predictor terms was analyzed for the continuous predictors (See Table 2 for predictors description).

Predictor	Statistic	Internal validation			Model interpolation			Model extrapolation		
		Linear	Quad	Cubic	Linear	Quad	Cubic	Linear	Quad	Cubic
Climatic										
MAT	R^2	0.03	0.07	0.09	0.03	0.07	0.09	0.07	0.07	0.04
	nRMSE	17.61	17.21	17.03	17.59	17.19	17.01	17.66	17.20	17.51
AP	R^2	0.07	0.12	0.12	0.07	0.12	0.12	0.07	0.08	0.08
	nRMSE	17.22	16.72	16.72	17.20	16.74	16.73	17.26	17.37	17.38
TS	R^2	0.04	0.04	0.05	0.04	0.04	0.05	0.06	0.07	0.05
	nRMSE	17.49	17.47	17.39	17.47	17.46	17.38	17.95	17.95	17.88
PS	R^2	0.02	0.03	0.06	0.02	0.03	0.06	0.03	0.04	0.04
	nRMSE	17.65	17.57	17.30	17.62	17.55	17.28	17.88	17.74	17.74
MTDQ	R^2	0.05	0.09	0.09	0.05	0.09	0.09	0.07	0.07	0.06
	nRMSE	17.34	16.99	16.98	17.32	16.98	16.97	17.44	17.57	17.66
PDQ	R^2	0.04	0.09	0.10	0.04	0.09	0.10	0.05	0.04	0.06
	nRMSE	17.49	17.02	16.88	17.46	17.03	16.87	17.55	17.65	17.48
Topographic										
Slope	R^2	0.02	0.02	0.02	0.02	0.03	0.03	0.01	0.02	0.02
	nRMSE	17.69	17.62	17.62	17.66	17.59	17.58	18.05	17.92	17.92
TPI	R^2	0.00	0.00	0.01	0.01	0.01	0.01	0.00	0.00	0.01
	nRMSE	17.80	17.79	17.79	17.75	17.75	17.75	18.13	18.15	18.10
TCI	R^2	0.00	0.01	0.01	0.01	0.01	0.01	0.01	0.01	0.01
	nRMSE	17.79	17.79	17.79	17.76	17.75	17.75	18.11	18.10	18.10
HL	R^2	0.00	0.01	0.01	0.00	0.01	0.01	0.00	0.00	0.01
	nRMSE	17.81	17.78	17.78	17.78	17.75	17.75	18.11	18.11	18.10
Fuel load-type										
GLC class	R^2	0.09	–	–	0.09	–	–	0.03	–	–
	nRMSE	17.03	–	–	17.02	–	–	18.21	–	–
FAPAR	R^2	0.23	0.27	0.28	0.22	0.27	0.27	0.13	0.17	0.19
	nRMSE	15.70	15.22	15.18	15.71	15.22	15.19	16.78	16.24	16.10
LAI	R^2	0.22	0.27	0.29	0.21	0.26	0.28	0.09	0.13	0.14
	nRMSE	15.79	15.20	15.07	15.79	15.28	15.09	17.40	17.04	16.90
FCOV	R^2	0.24	0.27	0.27	0.23	0.26	0.26	0.08	0.11	0.11
	nRMSE	15.58	15.27	15.27	15.62	15.28	15.27	17.44	17.16	17.15
Fuel load-moisture										
NDWI	R^2	0.27	0.3	0.33	0.27	0.30	0.32	0.19	0.21	0.23
	nRMSE	15.23	14.92	14.65	15.27	14.95	14.69	16.17	15.86	15.71
MSI	R^2	0.21	0.21	0.22	0.21	0.21	0.22	0.11	0.11	0.12
	nRMSE	15.83	15.83	15.75	15.83	15.83	15.74	16.89	16.88	16.85
CWC	R^2	0.16	0.20	0.21	0.15	0.20	0.21	0.05	0.05	0.05
	nRMSE	16.35	15.93	15.87	16.38	15.94	15.87	17.73	17.73	17.71
CR	R^2	0.02	0.03	0.03	0.03	0.03	0.03	0.03	0.03	0.03
	nRMSE	17.62	17.59	17.58	17.58	17.56	17.55	17.92	17.90	17.90
Fuel continuity										
Patch size	R^2	0.02	0.02	0.02	0.02	0.02	0.02	0.00	0.00	0.00
	nRMSE	17.68	17.65	17.65	17.65	17.62	17.63	18.09	18.09	18.11
FCOV homog	R^2	0.01	0.02	0.02	0.01	0.01	0.01	0.01	0.00	0.00
	nRMSE	17.76	17.70	17.70	17.73	17.69	17.69	18.44	18.38	18.39

Table 4
Results of internal validation (fitting of model predictions to the training data), interpolation (fitting of model predictions to independent data within the training wildfires) and extrapolation (fitting of model predictions to data from independent wildfires) of the Random Forest models performed with each group of environmental variables (climatic: MAT, AP, TS, PS, MTDQ, PDQ; topographic: Slope, TPI, TCI, HL; fuel load-type: GLC class, FAPAR, LAI, FCOV; fuel load-moisture: NDWI, MSI, CWC, CR; and fuel continuity: Patch size and FCOV homogeneity).

Group	Statistic	Internal validation	Model interpolation	Model extrapolation
Climatic	R^2	0.41	0.37	0.05
	nRMSE	13.71	14.14	20.52
Topographic	R^2	0.77	0.05	0.03
	nRMSE	11.28	17.43	17.89
Fuel load-type	R^2	0.57	0.32	0.22
	nRMSE	12.07	14.74	16.17
Fuel load-moisture	R^2	0.81	0.33	0.20
	nRMSE	8.78	14.63	16.16
Fuel continuity	R^2	0.53	0.14	0.00
	nRMSE	13.01	16.61	20.25

productivity, and thereby on fuel accumulation. In addition, we found that the driest and most seasonal sites exhibited the lowest severities, which could be interpreted as opposite to the assumptions that relate climate warming to increases in wildfire severity, due to enhancing fuel aridity and lengthening of the fire season (Stephens et al., 2013; Abatzoglou et al., 2019; Keeley et al., 2019; Moreira et al., 2020). However, previous work has demonstrated that the effects of climate warming on fire behavior must be analyzed from a broader perspective, as over the long term climate might drive not only fuel conditions but also fuel amount (Rogers et al., 2020), fire frequency, the efficacy of suppression efforts, and even cause the replacement of ecosystems by others with different associated severities (Rogers et al., 2011). In this context, McKenzie and Littell (2017) found that increases in burned area with climate warming are expected mainly in ecosystems with intermediate water-balance deficits, which are those in the middle of the flammability-limited to fuel-limited fire regime gradient.

Individually, topographic variables were weakly related to burn severity, mainly affected by slope, which showed that burn severity increases with steepness between 0 and 15°. These results agreed with Fang et al. (2019), who identified slope as the most important topographic variable driving burn severity. Slope may increase wildfire severity by regulating vegetation composition and amount, facilitating drainage, influencing

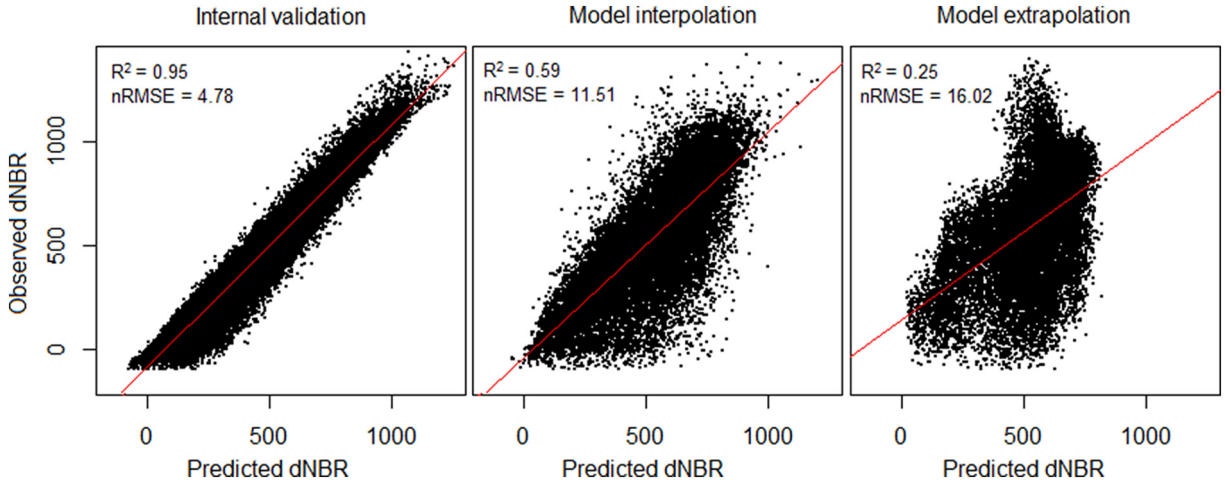

Fig. 4. Scatterplots showing the results of internal validation (fitting of model predictions to the training data), interpolation (fitting of model predictions to independent data within the training wildfires) and extrapolation (fitting of model predictions to data from independent wildfires) of the full random forest model.

solar exposure, wildfire spread, and, in upslope fires, facilitating preheating on the adjacent fuels which increases wildfire severity (Lentile et al., 2009; Kane et al., 2015; Fang et al., 2019; García-Llamas et al., 2019a).

It is known that continuous large amounts of fuel can lead to high severity fires (Collins et al., 2007; Stephens et al., 2013; Moreira et al., 2020). However, our results did not show strong relationships between fuel continuity and burn severity. This indicates the necessity of combining continuity variables with other fuel properties, such as fuel load, to obtain a meaningful predictor of burn severity, as equal values of fuel homogeneity (patch size or FCOV homogeneity) can be obtained in bare areas and in densely vegetated zones if spatial variability is the same.

4.2. Performance of predictive models of burn severity

Some of the developed machine-learning models showed a high predictive capacity (root mean square errors <12% and 59% of variance explained) when applied to independent data. This represents a substantial improvement over models developed to predict continuous severity data so far, which have been able to explain up to 43% of severity variance when applied to independent data within the same wildfires (Birch et al., 2015; García-Llamas et al., 2019a, 2019b). Nonetheless, the predictive capacity of models largely varied depending on the set of predictors and the dataset on which the predictions were applied.

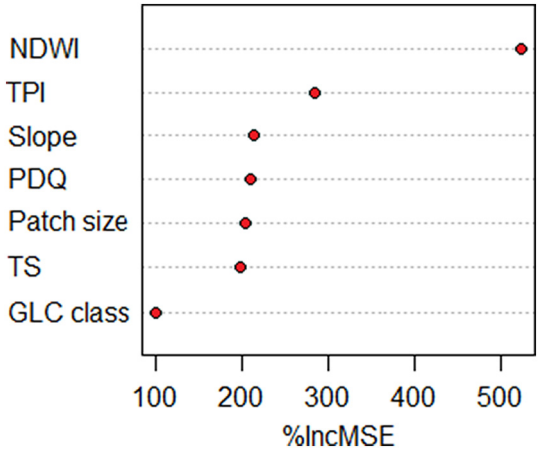

Fig. 5. Relative importance, measured as percentage increase in mean square error (%IncMSE), of each feature from the parsimonious random forest model when predicting burn severity. NDWI: Pre-burn NDWI index, TPI: Topographic Position Index, PDQ: Precipitation of Driest Quarter, TS: Temperature Seasonality, GLC Class: Copernicus Global Land Cover class.

Models performed using groups of variables outperformed the predictive capacity of most individual variables, and both were largely surpassed by the comprehensive models combining the studied groups of predictors (full and parsimonious). This is in accordance with previous results found in the Iberian Peninsula (García-Llamas et al., 2019a) and in Western United States (Birch et al., 2015), and reflects two aspects, firstly the different contribution of the studied variables to explain the burn severity variance and to enhance predictive capacity; and secondly, the convenience of considering the complex interactions between variables, which was manifested by the importance acquired in the comprehensive models by variables that, individually, were poorly effective in predicting burn severity. This was the case of most climatic, topographic and fuel homogeneity variables, as their effects on burn severity vary depending on fuel characteristics (Rogers et al., 2011, 2020). Comparing the full and parsimonious models both showed similar performance, as found by García-Llamas et al. (2019a). Moreover, the retention of climate (PDQ, TS), topographic (TPI, Slope), fuel load-type (GLC class), fuel load-moisture (NDWI) and fuel continuity (Patch size) variables in the parsimonious RF model reveals that all types of variables are somehow important in predicting burn severity.

Our study is the first to analyze the potential generalization of burn severity predictive models, demonstrating that interpolations, and particularly extrapolations with high predictive capacity remain a challenge. In terms of model extrapolation, the NDWI, the full and the parsimonious RF models showed similar predictive capacities, suggesting that both NDWI and the parsimonious RF model are the less time-consuming and the most operational alternatives for decision-making. The loss of predictive capacity of models when applied to other study sites is the expected pattern (Sequeira et al., 2018), and can be a consequence of uncertainties related to satellite imagery dates and pre-processing (Fernández-Guisuraga et al., 2020), or of insufficient retrieval in the training data of all the potential conditions influencing the response variable (Werkowska et al., 2016; Sequeira et al., 2018). In this sense, and to advance in the prediction of burn severity, we suggest for future work (i) to consider the influence of fire suppression actions on fire severity, not considered in this study because the lack of available spatial data; (II) To use a higher amount of data from diverse burned areas and capturing even more heterogeneous situations, as each burned patch is characterized by particular combinations of environmental conditions that should be considered in model training; (III) To include dynamic variables related to fire-weather at the synoptic scale (Jolly et al., 2015; Abatzoglou et al., 2019), as extreme weather conditions may overwhelm the influence of landscape-scale variables

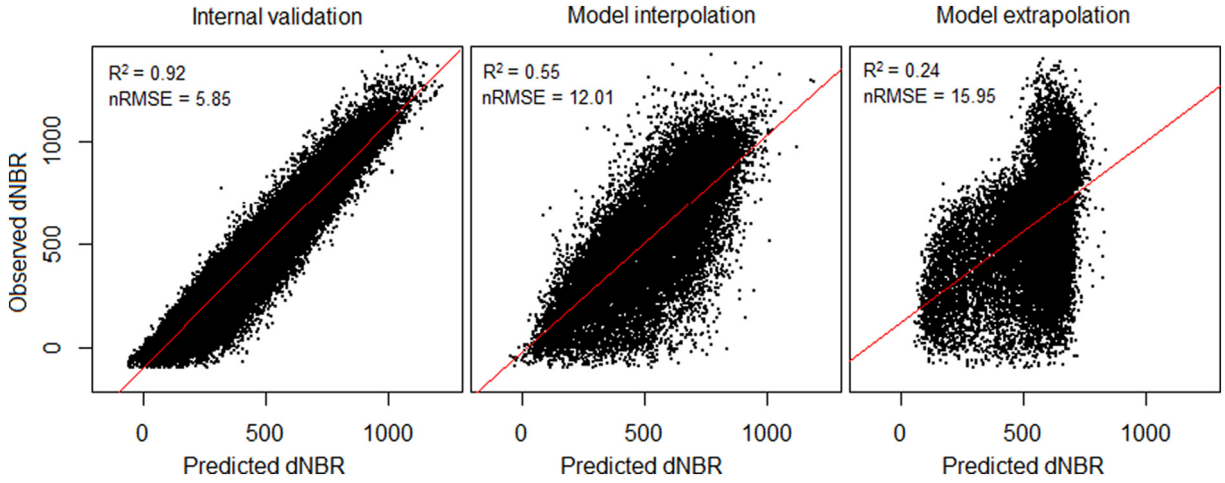

Fig. 6. Scatterplots showing the results of internal validation (fitting of model predictions to the training data), interpolation (fitting of model predictions to independent data within the training wildfires) and extrapolation (fitting of model predictions to data from independent wildfires) of the parsimonious random forest model.

(Prichard et al., 2020); (IV) To engage dynamic heat transfer models at the local scale, as they have shown to drive fire spread and intensity (Morandini and Silvani, 2010); and (V) to consider the vertical fuel structure that significantly determine burn severity (Fang et al., 2018; Fernández-Guisuraga et al., 2021) would be useful to enhance predictions and may contribute to increasing the generalization capacity of burn severity predictive models. The characterization of fuel vertical structure has been largely addressed at the local and regional scale using LiDAR data (Matasci et al., 2018; Fernández-Guisuraga et al., 2021) because global data sources did not formerly exist. However, the recently launched GEDI instrument opens the opportunity to incorporate lidar data in future predictive models of burn severity in southern Europe as it is anticipated that 4% of the Earth's land surface will be sampled (51.6°N and 51.6°S latitudes) over a nominal two-year mission (Potapov et al., 2021).

4.3. Management implications

The results of the present study provide managers with predictive severity models based on landscape-scale variables that outperform former state-of-art models (Birch et al., 2015; García-Llamas et al., 2019a, 2019b), which in addition have the potential of being applicable worldwide because of the use of global data sources. The application of these models is key to identifying areas where fire danger is critical in terms of burn severity, and provide insights on how climate change might affect burn severity.

Our study also contributes to the design of the pre-fire management strategies to mitigate burn severity, demonstrating that manageable fuel-related variables are primary drivers of burn severity, and specifically fuel load, which is closely linked to vegetation cover, leaf area, photosynthetic activity and moisture. Moreover, we identified dense coniferous and shrubs as the most prone land cover classes to severe fires, probably because of their proneness to burn most of the plant aerial biomass (Keeley et al., 2011). In accordance, management aimed at reducing high severity danger should pursue a reduction in fuel accumulation (Moreira et al., 2011), mainly in density of coniferous forest and shrublands, and crown fire likelihood, with actions such as thinning, clearing, pruning, or even the combination of thinning with prescribed burning (Kalies and Yocom Kent, 2016). Previous work (Agee and Skinner, 2005) also indicates that the reduction of surface fuels, the retention of large trees of fire-resistant species are effective actions for reducing the risk of severe fire. A periodical assessment is advisable after these silvicultural treatments, as open forests may facilitate the development of a dense shrubby understory (Fernandes and Rigolot, 2007).

5. Conclusions

This study contributes to advancements in the fire ecology and environmental management disciplines by providing models applicable anywhere in the world thanks to the use of global data sources, and with a greater capacity to predict continuous burn severity values than those developed to date.

Moreover, we conclude that burn severity is closely related to variables from multispectral data related to fuel load, such as the NDWI index, although climatic, topographic and fuel continuity variables are also important to enhance predictive models.

Moreover, this study, which is pioneer in analyzing the generalization capacity of predictive models of burn severity, reveals that model extrapolation to independent regions causes a drop in the model performance, which might be addressed using a larger amount of training data in order to capture all potential fire conditions and environmental situations, and by the consideration of further predictors that affect fire behavior and severity.

Finally, on the basis of our results we identified target areas for management as those with high fuel load, particularly closed coniferous forests and shrublands. In these areas, management actions aimed at reducing susceptibility to severe fires should be designed to reduce fuel load, density of trees and shrubs and proneness to crown fires.

Funding

This study was financially supported by the Spanish Ministry of Economy and Competitiveness, and the European Regional Development Fund (ERDF) in the framework of the FIRESEVES project [grant number AGL2017-86075-C2-1-R] and by the Regional Government of Castile and León in the framework of the WUIFIRECYL project [grant number LE005P20]. Víctor Fernández-García is supported by a Margarita Salas post-doctoral fellowship from the Ministry of Universities, financed with European Union-NextGenerationEU funds granted by the University of León, David Beltrán-Marcos is supported by a pre-doctoral fellowship from the Regional Government of Castile and León [EDU/ 556/2019] and José Manuel Fernández-Guisuraga is supported by a post-doctoral contract under the WUIFIRECYL project [LE005P20].

Authors responsibilities

VF-G and LC conceptualization; VF-G, DB-M and JMF-G data acquisition; VF-G design of the original draft, data curation, formal analysis, methodology, validation, and writing; LC funding acquisition and project

administration; LC and EC supervision; VF-G DB-M, JF-G, EM and LC review & editing.

Declaration of competing interest

The authors declare that they have no known competing financial interests or personal relationships that could have appeared to influence the work reported in this paper.

Appendix A. Supplementary data

Supplementary data to this article can be found online at https://doi.org/10.1016/j.scitotenv.2022.154729.

References

Abatzoglou, J.T., Williams, A.P., Barbero, R., 2019. Global emergence of anthropogenic climate change in fire weather indices. Geophys. Res. Lett. 46, 326–336. https://doi.org/10.1029/2018GL080959.

Agee, J.K., Skinner, C.N., 2005. Basic principles of forest fuel reduction treatments. For. Ecol. Manag. 211, 83–96. https://doi.org/10.1016/j.foreco.2005.01.034.

Alonso-González, E., Fernández-García, V., 2021. MOSEV: a global burn severity database from MODIS (2000–2020). Earth Syst. Sci. Data 13, 1925–1938. https://doi.org/10.5194/essd-13-1925-2021.

Babu, K.V., Roy, A., Prasad, P.R., 2015. Fire Potential Index for Uttarakhand using Daily MODIS TERRA satellite datasets. OSGIS-2015, pp. 89–97.

Birch, D.S., Morgan, P., Kolden, C.A., Abatzoglou, J.T., Dillon, G.K., Hudak, A.T., Smith, A.M.S., 2015. Vegetation, topography and daily weather influenced burn severity in central Idaho and western Montana forests. Ecosphere 6, 1–23. https://doi.org/10.1890/ES14-00213.1.

Buchhorn, M., Smets, B., Bertels, L., De Roo, B., Lesiv, M., Tsendbazar, N.E., Herold, M., Fritz, S., 2020. Copernicus Global Land Service: Land Cover 100m: Collection 3: epoch 2015: Globe. https://doi.org/10.5281/zenodo.3939038.

Chu, T., Guo, X., 2014. Remote sensing techniques in monitoring post-fire effects and patterns of forest recovery in boreal forest regions: a review. Remote Sens. 6, 470–520. https://doi.org/10.3390/rs6010470.

Chuvieco, E., Riaño, D., Danson, F.M., Martin, P., 2006. Use of a radiative transfer model to simulate the postfire spectral response to burn severity. J. Geophys. Res. 111, G04S09. https://doi.org/10.1029/2005JG000143.

CLC, 2012. Corine Land Cover, 2012 Version 2020_20u1. https://land.copernicus.eu/pan-european/corine-land-cover/clc-2012 (accessed 1 December 2021).

CLC, 2018. Corine Land Cover, 2018, Version 2020_20u1. https://land.copernicus.eu/pan-european/corine-land-cover/clc2018?tab=metadata (accessed 1 December 2021).

Coen, J.L., Cameron, M., Michalakes, J., Patton, E.G., Riggan, P.J., Yedinak, K.M., 2013. WRF-fire: coupled weather–wildland fire modeling with the weather research and forecasting model. J. Appl. Meteorol. Climatol. 52, 16–38. https://doi.org/10.1175/JAMC-D-12-023.1.

De Santis, A., Chuvieco, E., Vaughan, P.J., 2009. Short-term assessment of burn severity using the inversion of PROSPECT and GeoSail models. Remote Sens. Environ. 113, 126–136. https://doi.org/10.1016/j.rse.2008.08.008.

Dillon, G.K., Holden, Z.A., Morgan, P., Crimmins, M.A., Heyerdahl, E.K., Luce, C.H., 2011. Both topography and climate affected forest and woodland burn severity in two regions of the western US, 1984 to 2006. Ecosphere 2, 130. https://doi.org/10.1890/ES11-00271.1.

Dilts, T.E., 2015. Topography Tools for ArcGIS 10.1. University of Nevada Reno. http://www.arcgis.com/home/item.html?id=b13b3b40fa3c43d4a23a1a09c5fe96b9 (accessed 1 December 2021).

Diniz-Filho, J.A., Siquiera, T., Padial, A.A., Rangel, T.F., Landeiro, V.L., Bini, L.M., 2012. Spatial autocorrelation analysis allows disentangling the balance between neutral and niche processes in metacommunities. Oikos 121, 201–210. https://doi.org/10.1111/j.1600-0706.2011.19563.x.

Doherty, T.S., Davis, R.A., van Etten, E.J.B., Collier, N., Krawiec, J., 2015. Response of a shrubland mammal and reptile community to a history of landscape-scale wildfire. Int. J. Wildland Fire 24, 534–543. https://doi.org/10.1071/WF14115.

Dupuy, J.L., Marechal, J., Portier, D., Valette, J.-C., 2011. The effects of slope and fuel bed width on laboratory fire behaviour. Int. J. Wildland Fire 20, 272–288. https://doi.org/10.1071/WF09075.

ESA, 2021. Sentinel-1 SAR User Guide. European Space Agency. https://sentinel.esa.int/web/sentinel/user-guides/sentinel-1-sar (accessed 1 December 2021).

ESRI, 2019. ArcGIS Release 10.7. https://desktop.arcgis.com/.

Exelis Visual Information Solutions, Inc., a subsidiary of Harris Corporation, 2015. ENVI 5.3 (Version 5.3). http://www.harrisgeospatial.com/ProductsandSolutions/GeospatialProducts.aspx.

Fang, L., Yang, J., White, M., Liu, Z., 2018. Predicting potential fire severity using vegetation, topography and surface moisture availability in a eurasian boreal forest landscape. Forests 9, 130. https://doi.org/10.3390/f9030130.

Fernandes, P.M., Rigolot, E., 2007. The fire ecology and management of maritime pine (*Pinus pinaster* Ait.). For. Ecol. Manag. 241, 1–13. https://doi.org/10.1016/j.foreco.2007.01.010.

Fernández-García, V., Santamarta, M., Fernández-Manso, A., Quintano, C., Marcos, E., Calvo, L., 2018. Burn severity metrics in fire-prone pine ecosystems along a climatic gradient using Landsat imagery. Remote Sens. Environ. 206, 205–217. https://doi.org/10.1016/j.rse.2017.12.029.

Fernández-García, V., Fulé, P.Z., Marcos, E., Calvo, L., 2019a. The role of fire frequency and severity on the regeneration of Mediterranean serotinous pines under different environmental conditions. For. Ecol. Manag. 444, 59–68. https://doi.org/10.1016/j.foreco.2019.04.040.

Fernández-García, V., Marcos, E., Fernández-Guisuraga, J.M., Taboada, A., Suárez-Seoane, S., Calvo, L., 2019b. Impact of burn severity on soil properties in a *Pinus pinaster* ecosystem immediately after fire. Int. J. Wildland Fire 28, 354–364. https://doi.org/10.1071/WF18103.

Fernández-García, V., Marcos, E., Fulé, P.Z., Reyes, O., Santana, V., Calvo, L., 2020. Fire regimes shape diversity and traits of vegetation under different climatic conditions. Sci. Total Environ. 716, 137137. https://doi.org/10.1016/j.scitotenv.2020.137137.

Fernández-García, V., Marcos, E., Huerta, S., Calvo, L., 2021. Soil-vegetation relationships in Mediterranean forests after fire. For. Ecosyst. 8, 18. https://doi.org/10.1186/s40663-021-00295-y.

Fernández-Guisuraga, J.M., Calvo, L., Fernández-García, V., Marcos-Porras, E., Taboada, A., Suárez-Seoane, S., 2019. Efficiency of remote sensing tools for post-fire management along a climatic gradient. For. Ecol. Manag. 433, 553–562. https://doi.org/10.1016/j.foreco.2018.11.045.

Fernández-Guisuraga, J.M., Suárez-Seoane, S., García LLamas, P., Calvo, L., 2021. Vegetation structure parameters determine high burn severity likelihood in different ecosystem types: a case study in a burned Mediterranean landscape. J. Environ. Manag. 288, 112462. https://doi.org/10.1016/j.jenvman.2021.112462.

Fernández-Manso, A., Quintano, C., Roberts, D.A., 2020. Can Landsat-derived variables related to energy balance improve understanding of burn severity from current operational techniques? Remote Sens. 12, 890. https://doi.org/10.3390/rs12050890.

Fick, S.E., Hijmans, R.J., 2017. WorldClim 2: new 1km spatial resolution climate surfaces for global land areas. Int. J. Climatol. 37, 4302–4315. https://doi.org/10.1002/joc.5086.

García-Llamas, P., Suárez-Seoane, S., Taboada, A., Fernández-Manso, A., Quintano, C., Fernández-García, V., Fernández-Guisuraga, J.M., Marcos-Porras, E., Calvo, L., 2019a. Environmental drivers of fire severity in extreme fire events that affect Mediterranean pine forest ecosystems. For. Ecol. Manag. 433, 24–32. https://doi.org/10.1016/j.foreco.2018.10.051.

García-Llamas, P., Suárez-Seoane, S., Taboada, A., Fernández-García, V., Fernández-Guisuraga, J.M., Fernández-Manso, A., Quintano, C., Marcos-Porras, E., Calvo, L., 2019b. Assessment of the influence of biophysical properties related to fuel conditions on fire severity using remote sensing techniques: a case study on a large fire in NW Spain. Int. J. Wildland Fire 28, 512–520. https://doi.org/10.1071/WF18156.

García-Llamas, P., Suárez-Seoane, S., Fernández-Guisuraga, J.M., Fernández-García, V., Fernández-Manso, A., Quintano, C., Taboada, A., Marcos-Porras, E., Calvo, L., 2019c. Evaluation and comparison of Landsat 8, Sentinel-2 and Deimos-1 remote sensing indices for assessing burn severity in Mediterranean fire-prone ecosystems. Int. J. Appl. Earth Obs. Geoinf. 80, 137–144. https://doi.org/10.1016/j.jag.2019.04.006.

Gómez-Sánchez, E., de las Heras, J., Lucas-Borja, M., Moya, D., 2017. Assessing fire severity in semi-arid environments: application in Donceles 2012 wildfire (SE Spain). Revista de Teledetección 49, 103–113. https://doi.org/10.4995/raet.2017.7121.

Hallema, D.W., Sun, G., Caldwell, P.V., Norman, S.P., Cohen, E.C., Liu, Y., Bladon, K.D., McNulty, S.G., 2018. Burned forests impact water supplies. Nat. Commun. 9, 1307. https://doi.org/10.1038/s41467-018-03735-6.

Han, A., Qing, S., Bao, Y., Na, L., Bao, Y., Liu, X., Zhang, J., Wang, C., 2021. Short-term effects of fire severity on vegetation based on Sentinel-2 satellite data. Sustainability 13, 432. https://doi.org/10.3390/su13010432.

Jenness, J., 2006. Topographic Position Index (tpi_jen.avx) extension for ArcView 3.x. (Version 1.3a). http://www.jennessent.com/arcview/tpi.htm.

Jolly, W., Cochrane, M., Freeborn, P., Holden, Z.A., Brown, T., Williamson, G.J., Bowman, D.M.J.S., 2015. Climate-induced variations in global wildfire danger from 1979 to 2013. Nat. Commun. 6, 7537. https://doi.org/10.1038/ncomms8537.

Kalabodikis, K., Palaiologou, P., 2019. Mediterranean Forest Fuels. Encyclopedia of Wildfires and Wildland-Urban Interface (WUI) Fires. https://doi.org/10.1007/978-3-319-51727-8_29-1.

Kalies, E.L., Yocom Kent, L.L., 2016. Tamm Review: are fuel treatments effective at achieving ecological and social objectives? A systematic review. For. Ecol. Manag. 375, 84–95. https://doi.org/10.1016/j.foreco.2016.05.021.

Kane, V.R., Lutz, J.A., Cansler, C.A., Povak, N.A., Churchill, D.J., Smith, D.F., Kane, J.T., North, M.P., 2015. Water balance and topography predict fire and forest structure patterns For. For. Ecol. Manag. 338, 1–13. https://doi.org/10.1016/j.foreco.2014.10.038.

Keeley, J.E., 2009. Fire intensity, fire severity and burn severity: a brief review and suggested usage. Int. J. Wildland Fire 18, 116–126. https://doi.org/10.1071/WF07049.

Keeley, J.E., Bond, W.J., Bradstock, R.A., Pausas, J.G., Rundell, P.W., 2011. Fire in Mediterranean Ecosystems: Ecology. Cambridge University Press, Cambridge, Evolution and Management https://doi.org/10.1017/CBO9781139033091.

Keeley, J.E., van Mantgem, P., Falk, D.A., 2019. Fire, climate and changing forests. Nat. Plants 5, 774–775. https://doi.org/10.1038/s41477-019-0485-x.

Key, C.H., Benson, N.C., 2006. Landscape assessment (LA) sampling and analysis methods. USDA Forest Service General Technical Report, RMRS-GTR-164-CD.

Kraaij, T., Baard, J.A., Arndt, J., Vhengani, L., van Wilgen, B.W., 2018. An assessment of climate, weather, and fuel factors influencing a large, destructive wildfire in the Knysna region, South Africa. Fire Ecol. 14, 4. https://doi.org/10.1186/S42408-018-0001-0.

Krawchuk, M.A., Moritz, M.A., 2011. Constraints on global fire activity vary across a resource gradient. Ecology 92, 121–132. https://doi.org/10.1890/09-1843.1.

Kremer, L.P.M., Anders, S., 2019. Package 'ggpointdensity' (Version 0.1.0). https://cran.r-project.org/web/packages/ggpointdensity/ggpointdensity.pdf.

Kuhn, M., 2008. Building predictive models in R using the caret package. J. Stat. Softw. 28, 1–26. https://doi.org/10.18637/jss.v028.i05.

Lee, H.J., Choi, Y.E., Lee, S.W., 2018. Complex relationships of the effects of topographic characteristics and susceptible tree cover on burn severity. Sustainability 10, 295. https://doi.org/10.3390/su10020295.
Liaw, A., Wiener, M., 2002. Classification and regression by randomForest. R News 2, 18–22.
Loehman, R.A., 2020. Drivers of wildfire carbon emissions. Nat. Clim. Chang. 10, 1070–1071. https://doi.org/10.1038/s41558-020-00922-6.
López-García, M.J., Caselles, V., 1991. Mapping burns and natural reforestation using thematic mapper data. Geocarto Int. 1, 31–37. https://doi.org/10.1080/10106049109354290.
McCune, B., Keon, D., 2002. Equations for potential annual direct incident radiation and heat load. J. Veg. Sci. 13, 603–606. https://doi.org/10.1111/j.1654-1103.2002.tb02087.x.
McKenzie, D., Littell, J.S., 2017. Climate change and the eco-hydrology of fire: will area burned increase in a warming western USA? Ecol. Appl. 27, 26–36. https://doi.org/10.1002/eap.1420.
Meyer, F., 2019. Spaceborne synthetic aperture radar – principles, data access, and basic processing techniques. In: Flores, A., Herndon, K., Thapa, R., Cherrington, E. (Eds.), SAR Handbook: Comprehensive Methodologies for Forest Monitoring and Biomass Estimation. NASA, Huntsville, pp. 21–64 https://doi.org/10.25966/ez4f-mg98.
Mitsopoulos, I., Chrysafi, I., Bountis, D., Mallinis, G., 2019. Assessment of factors driving high fire severity potential and classification in a Mediterranean pine ecosystem. J. Environ. Manag. 235, 266–275. https://doi.org/10.1016/j.jenvman.2019.01.056.
Morandini, F., Silvani, X., 2010. Experimental investigation of the physical mechanisms governing the spread of wildfires. Int. J. Wildland Fire 19, 570–582. https://doi.org/10.1071/WF08113.
Moreira, F., Viedma, O., Arianoutsou, M., Curt, T., Koutsias, N., Rigolot, E., Barbati, A., Corona, P., Vaz, P., Xanthopoulos, G., Mouillot, F., Bigili, E., 2011. Landscape – wildfire interactions in southern Europe: Implications for landscape management. J. Environ. Manag. 92, 2389–2402. https://doi.org/10.1016/j.jenvman.2011.06.028.
Moreira, F., Ascoli, D., Safford, H., Adams, M.A., Moreno, J.M., Pereira, J.M., Catry, F.X., Armesto, J., Bond, W., González, M.E., Curt, T., Koutsias, N., McCaw, L., Price, O., Pausas, J.G., Rigolot, E., Stephens, S., Tavsanoglu, C., Vallejo, V.R., Van Wilgen, B.W., Xanthopoulos, G., Fernandes, P.M., 2020. Wildfire management in Mediterranean-type regions: paradigm change needed. Environ. Res. Lett. 15, 011001. https://doi.org/10.1088/1748-9326/ab541e.
Myers, N., Mittermeier, R., Mittermeier, C., Fonseca, G.A.B., Kent, J., 2000. Biodiversity hotspots for conservation priorities. Nature 403, 853–858. https://doi.org/10.1038/35002501.
Connor, C.D.O'., Calkin, D.E., Thompson, M.P., 2017. An empirical machine learning method for predicting potential fire control locations for pre-fire planning and operational fire management. Int. J. Wildland Fire 26, 587–597. https://doi.org/10.1071/WF16135.
Parks, S.A., Miller, C., Abatzoglou, J.T., Holsinger, L.M., Parisien, M.A., Dobrowski, S.Z., 2016. How will climate change affect wildland fire severity in the western US? Environ. Res. Lett. 11, 035002. https://doi.org/10.1088/1748-9326/11/3/035002.
Pasqualotto, N., D'Urso, G., Falanga Bolognesi, S., Rosario Belfiore, O., Van Wittenberghe, S., Delegido, J., Pezzola, A., Winschel, C., Moreno, J., 2019. Retrieval of evapotranspiration from Sentinel-2: comparison of vegetation indices, semi-empirical models and SNAP biophysical processor approach. Agronomy 9, 663. https://doi.org/10.3390/agronomy9100663.
Pausas, J.G., Llovet, J., Rodrigo, A., Vallejo, R., 2008. Are wildfires a disaster in the Mediterranean basin? – A review. Int. J. Wildland Fire 17, 713–723. https://doi.org/10.1071/WF07151.
Potapov, P., Li, X., Hernández-Serna, A., Tyukavina, A., Hansen, M.C., Kommareddy, A., Pickens, A., Turubanova, S., Tang, H., Edibaldo, Silva C., Armston, J., Dubayah, R., Blair, J.B., Hofton, M., 2021. Mapping global forest canopy height through integration of GEDI and Landsat data. Remote Sens. Environ. 253, 112165. https://doi.org/10.1016/j.rse.2020.112165.
Prichard, S.J., Povak, N.A., Kennedy, M.C., Peterson, D.W., 2020. Fuel treatment effectiveness in the context of landform, vegetation, and large, wind-driven wildfires. Ecol. Appl. 30, 1–22. https://doi.org/10.1002/eap.2104.
Probst, P., Boulesteix, A., 2018. To tune or not tune the number of trees in Random Forest. J. Mach. Learn. Res. 18, 1–18.
Quintano, C., Fernández-Manso, A., Roberts, D., 2017. Burn severity mapping from Landsat MESMA fraction images and land surface temperature. Remote Sens. Environ. 190, 83–95. https://doi.org/10.1016/j.rse.2016.12.009.
R Core Team, 2021. R: A Language and Environment for Statistical Computing. R Foundation for Statistical Computing. https://www.R-project.org/.
Ribeiro, L.M., Viegas, D.X., Almeida, M., McGee, T.K., Pereira, M.G., Parente, J., Xanthopoulos, G., Leone, V., Mariano, G., Hardin, H., 2020. 2 - Extreme wildfires and disasters around the world: lessons to be learned. In: Tedim, F., Leone, V., McGee, T.K. (Eds.), Extreme Wildfire Events and Disasters. Elsevier Inc https://doi.org/10.1016/B978-0-12-815721-3.00002-3 (31-pp. 51).
Rogers, B.M., Neilson, R.P., Drapek, R., Lenihan, J.M., Wells, J.R., Bachelet, D., Law, B.E., 2011. Impacts of climate change on fire regimes and carbon stocks of the US Pacific Northwest. J. Geophys. Res. Biogeosci. 116, G03037. https://doi.org/10.1029/2011JG001695.
Rogers, B.M., Balch, J.K., Goetz, S.J., Lehmann, C.E.R., Turetsky, M., 2020. Focus on changing fire regimes: interactions with climate, ecosystems, and society. Environ. Res. Lett. 15, 030201. https://doi.org/10.1088/1748-9326/ab6d3a.
Saatchi, S., 2019. SAR methods for mapping and monitoring forest biomass. In: Flores, A., Herndon, K., Thapa, R., Cherrington, E. (Eds.), SAR Handbook: Comprehensive Methodologies for Forest Monitoring and Biomass Estimation. NASA, pp. 207–254 https://doi.org/10.25966/hbm1-ej07.
Sequeira, A.M.M., Bouchet, P.J., Yates, K.L., Mengersen, K., Caley, M.J., 2018. Transferring biodiversity models for conservation: Opportunities and challenges. Methods Ecol. Evol. 9, 1250–1264. https://doi.org/10.1111/2041-210X.12998.
SRTM, 2000. Shuttle Radar Topography Mission 1 Arc-Second Global. https://doi.org/10.5066/F7PR7TFT.
Stephens, S.L., Agee, J.K., Fulé, P.Z., North, M.P., Romme, W.H., Swetnam, T.W., Turner, M.G., 2013. Managing forests and fire in changing climates. Science 342, 41–42. https://doi.org/10.1126/science.1240294.
Tarboton, D., 1997. A new method for the determination of flow directions and upslope areas in grid digital elevation models. Water Resour. Res. 33, 309–319. https://doi.org/10.1029/96WR03137.
Van der Knijff, J.M., Jones, R.J.A., Montanarella, L., 2000. Soil Erosion Risk Assessment in Europe. EUR 19044 EN. European Comission. https://esdac.jrc.ec.europa.eu/content/soil-erosion-risk-assessment-europe.
Veraverbeke, S., Lhermitte, S., Verstraeten, W.W., Goossens, R., 2010. The temporal dimension of differenced Normalized Burn Ratio (dNBR) fire/burn severity studies: the case of the large 2007 Peloponnese wildfires in Greece. Remote Sens. Environ. 114, 2548–2563. https://doi.org/10.1016/j.rse.2010.05.029.
Vreugdenhil, M., Wagner, W., Bauer-Marschallinger, B., Pfeil, I., Teubner, I., Rüdiger, C., Strauss, P., 2018. Sensitivity of Sentinel-1 backscatter to vegetation dynamics: an austrian case study. Remote Sens. 10, 1396. https://doi.org/10.3390/rs10091396.
Walker, X.J., Rogers, B.M., Veraverbeke, S., Johnstone, J.F., Baltzer, J.L., Barrett, K., Bourgeau-Chavez, L., Day, N.J., de Groot, W.J., Dieleman, C.M., Goetz, S., Hoy, E., Jenkins, L.K., Kane, E.S., Parisien, M.-A., Potter, S., Schuur, E.A.G., Turetsky, M., Whitman, E., Mack, M.C., 2020. Fuel availability not fire weather controls boreal wildfire severity and carbon emissions. Nat. Clim. Chang. 10, 1130–1136. https://doi.org/10.1038/s41558-020-00920-8.
Weiss, M., Baret, F., 2016. S2ToolBox level 2 Products: LAI, FAPAR. FCOVER, Institut National de la Recherche Agronomique (INRA), Avignon.
Werkowska, W., Márquez, A.L., Real, R., Acevedo, P., 2016. A practical overview of transferability in species distribution modeling. Environ. Rev. 25, 127–133. https://doi.org/10.1139/er-2016-0045.
Xie, Q., Dash, J., Huete, A., Jiang, A., Yin, G., Ding, Y., Peng, D., Hall, C.C., Brown, L., Shi, Y., Ye, H., Dong, Y., Huang, W., 2019. Retrieval of crop biophysical parameters from Sentinel-2 remote sensing imagery. Int. J. Appl. Earth Obs. Geoinf. 80, 187–195. https://doi.org/10.1016/j.jag.2019.04.019.